Revista Mexicana de Astronomía y Astrofísica, **39**, 311–330 (2003)

A STUDY OF THE VARIABILITY OF WATER MASER EMISSION IN A SAMPLE OF YOUNG STELLAR OBJECTS

M. A. Trinidad,[1] V. Rojas,[1] J. C. Plascencia,[2] A. Ricalde,[2] S. Curiel,[1] and L. F. Rodríguez[3]

Received 2003 April 21; accepted 2003 August 21

RESUMEN

Presentamos los resultados de observaciones de máseres de agua en una muestra de objetos estelares jóvenes. Las observaciones se hicieron usando la antena de 37 m de Haystack durante un periodo de tiempo de aproximadamente ocho meses. La muestra fue seleccionada para estudiar la variabilidad de la emisión de máseres de H_2O en fuentes jóvenes con luminosidades entre 260 y 2.5 $\times 10^4$ $L_\odot$. Los resultados se presentan en una serie de gráficas que permiten analizar la variación de la emisión máser y hacer una discusión de las propiedades globales de la muestra. Los resultados muestran que en todas las fuentes la emisión de máser de agua varía con el tiempo. En base a la variabilidad observada, la muestra presenta dos tipos de comportamiento. Aproximadamente la mitad de las fuentes muestran variaciones grandes en la intensidad de al menos una componente (mayor a un orden de magnitud) en intervalos de tiempo entre uno y varios meses, mientras que en todas las fuentes existe más de una componente donde los cambios en intensidad son mas pequeños (menor a un factor de 10) pero en escalas de tiempo similares. Finalmente, la variabilidad de la emisión máser observada no presenta un patrón de periodicidad claro en el tiempo y no encontramos una clara relación entre la luminosidad de las fuentes y la variabilidad de los máseres de agua. Desde un punto de vista estadístico, la variabilidad de los máseres de H_2O puede describirse como debida a pequeñas (10%) fluctuaciones Gaussianas en la opacidad de la línea.

ABSTRACT

We present results of water maser observations in a sample of young stellar objects. The observations were made using the Haystack 37 m antenna during a span of time of about eight months. The sample was selected to study the variability of the water maser emission in young sources with far-infrared luminosities between 260 and 2.5×10^4 $L_\odot$. The results are shown in a series of plots that allow the analysis of the variation of the maser emission and to discuss the global properties of the sample. The results show that in all the observed sources the water maser emission varies with time. Based on the observed variability, the sample shows two kinds of behavior. About half of the sources show large variations in the peak flux density of at least one feature (by more than an order of magnitude) in time spans between one and several months, while in all the sources there is more than one feature where the changes in peak flux density are smaller (by less than a factor of 10) but in similar time scales. Finally, the variability of the observed water maser emission does not show a clear periodicity pattern in time and we do not find a clear relationship between the luminosity of the sources and the water maser variability. From a statistical point of view, the H_2O maser variability can be described as due to small (10%) Gaussian fluctuations in the line opacity.

Key Words: **ISM: MOLECULES — MASERS — STARS:FORMATION**

[1]Instituto de Astronomía, Universidad Nacional Autónoma de México (UNAM), México, D. F., México.
[2]Facultad de Ciencias, UNAM, México, D. F., México.
[3]Centro de Radioastronomía y Astrofísica, UNAM, Morelia, Michoacán, México.

1. INTRODUCTION

One of the most exciting astrophysical phenomena is the powerful water maser emission found in relation to star-forming activity. Generally, water masers are a good indicator of the star-forming regions and their spectra show several features at different velocities. Currently, this non-thermal emission process has been used to study the innermost regions of some young stars (e.g., Furuya et al. 2000; Torrelles et al. 2001; Imai, Deguchi, & Sasao 2002) and can be used to understand the properties and physical conditions of the star-forming regions.

It is well known that H_2O maser emission, associated with Young Stellar Objects (YSOs), shows variability on short (days and weeks) and long (months and years) time scales. However, observations of water masers have focused on the distribution and proper motions of the masers associated with protostars (e.g., Claussen et al. 1998; Patel et al. 2000). Time variability studies of H_2O masers have been rather limited in scope, due to instrumental difficulties. Maser variability in YSOs has mainly been studied using single dish observations and only a few systematic surveys have been published so far (e.g,. Furuya et al. 2001; Valdettaro et al.Âž 2002).

In this work, we have used the 37 m Haystack antenna to study the H_2O maser variability in a sample of YSOs. The paper is organized as follows: the selection criteria of the sample are described in section § 2. In section § 3, we present the observations and data reduction procedure. The results are given in section § 4, and the discussion of the maser variability is presented in § 5. Finally, the main conclusions are given in § 6.

2. THE SAMPLE

The observed sources are located in star-forming regions and they are associated with YSOs. The selected sample of YSOs covers a variety of luminosities from 260 to 2.5×10^4 $L_\odot$. All the observed sources have previous detections of H_2O maser emission. The majority of the sources are known to have compact components at radio continuum wavelengths, and some of them are also associated with millimeter emission. In addition, the selected objects are associated with IRAS sources (or there is at least one IRAS source in the observed field), and they can be observed during long intervals of time in the northern hemisphere with the Haystack antenna.

In the present paper, we present the results of the best studied eleven sources in our sample, that is, those sources that were observed at five or more epochs. The main parameters of the selected sample are listed in Table 1, which contains: source name (column 1), position in B1950 coordinates (columns 2 and 3), systemic velocity (column 4), distance (column 5) and luminosity of the sources (column 6). The references for these parameters are given in the discussion.

3. OBSERVATIONS

The observations were made on several runs from December 2000 to July 2001 (in about one month intervals) using the Haystack 37 m radio telescope.[4] In addition, some sources were also observed in May and June, 1999. We operated remotely the antenna from the Instituto de Astronomía in Mexico City. We observed the maser transition $6_{16} \rightarrow 5_{23}$ at 22.235080 GHz of the H_2O molecule. The observations were made in position-switching mode with pairs of 5 minutes on-source integrations and 5 minutes off-source, and using a 4096 channel autocorrelator with a bandwidth of 17.8 MHz (~ 140 km s^{-1}). The beam size of the radio telescope was of $90''$ and the aperture efficiency was ~ 0.38 at the frequency of 22 GHz . The calibration of the telescope pointing was done by observing the planets Venus and Jupiter, as well as the strongest water maser in Cepheus. We estimate that the pointing accuracy is $\sim 10''$. All the spectra were corrected for atmospheric attenuation and for variations of the gain due to elevation. The data were edited and calibrated with the software package CLASS, using standard procedures.

4. RESULTS

Currently, there are few systematic studies of the water maser variability in star-forming regions. In the present paper, we intend to carry out a systematic study of a group of maser sources associated with YSOs. The main parameters of the water masers detected in our sample are listed in Table 2: source name (column 1), velocity range in which the maser emission was observed (columns 2 and 3), peak flux density (column 4) and the velocity of each maser component (column 5). In columns 6 and 7 the variability index and the variability rate of each water maser component are listed, respectively (see subsection 5.1). In columns 8 and 9, the maximum velocities of the blue (V_{blue}) and red (V_{red}) lobes of the CO outflow are listed. Some of the general properties of the detected maser features of the observed sources are described in the following subsections.

[4]Undergraduate Research at the Haystack Observatory of the Northeast Radio Observatory Corporation (NEROC) is supported by a grant from the National Science Foundation.

TABLE 1

PARAMETERS OF THE OBSERVED SOURCES

Source	Position (1950)		Velocity[a]	Distance	L_{FIR}
	α	δ	(km s^{-1})	(kpc)	(10^3 $L_\odot$)
AFGL5157	05 34 37.9	+31 57 51	−17.8	1.8	3.0
S233	05 35 51.2	+35 44 13	−17.2	1.8	6.4
AFGL5182	06 06 07.3	+21 51 12	−0.7	1.5	6.1
I20050+2720	20 05 01.2	+27 20 50	5.8	0.7	0.3
I20126+4104	20 12 41.0	+41 04 21	−3.8	1.6	8.5
S106FIR	20 25 32.4	+37 12 50	−1.1	0.6	10.4
AFGL2591	20 27 35.9	+40 01 15	−5.7	1.0	16.2
LkHα234	21 41 57.2	+65 53 08	−10.0	1.0	1.3
S140 IRS	22 17 41.0	+63 03 41	−6.5	0.9	23.6
CEPHEUS A	22 54 19.0	+61 45 46	−11.0	0.7	25.0
I23139+5939	23 13 58.9	+59 39 06	−44.7	3.5	12.8

[a]Cloud systemic velocity with respect to the LSR.

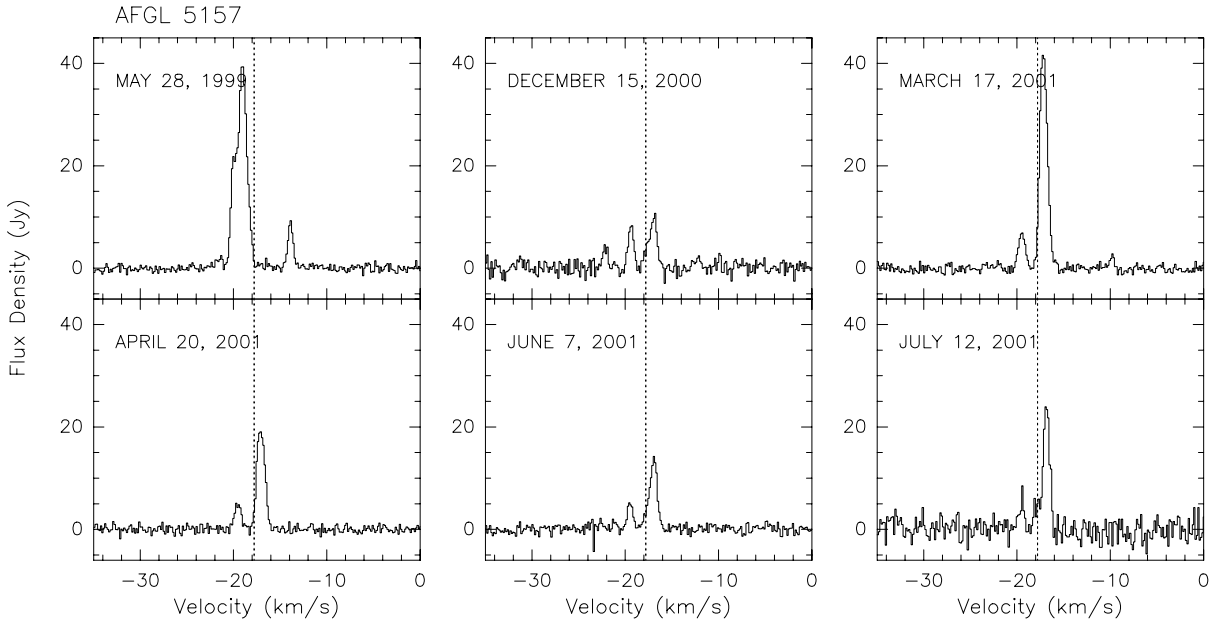

Fig. 1. Spectra of the detected H_2O maser toward the AFGL 5157 source. This figure shows the evolution of the water maser during a span of time of about six months. The horizontal axis is the LSR velocity (km s^{-1}), and the vertical axis is the peak flux density (Jy). Systemic velocity of the source is −17.8 km s^{-1} (vertical dashed line).

4.1. *AFGL 5157*

AFGL 5157 is located in the Perseus arm (Roberts 1972) and it is associated with a bipolar outflow (Snell et al. 1988). A radio continuum source associated with AFGL 5157 (Torrelles et al. 1992) and H_2O masers (Torrelles et al. 1992; Persi, Palagi, & Felli 1994) have been observed in this region. In addition, five possible HH objects seem to be located in the region.

The AFGL 5157 maser spectra are shown in Figure 1. The source was observed on six different occasions during a 775 day period, from May, 1999 to July, 2001. The majority of the spectra have only two maser features showing variability in their peak

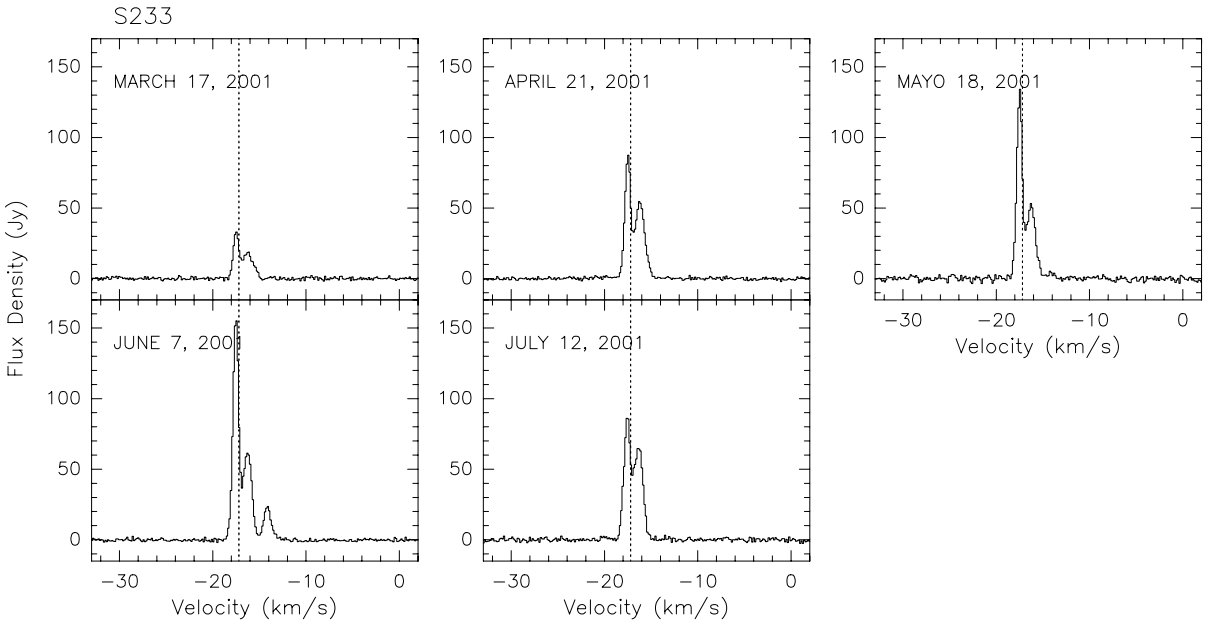

Fig. 2. Same as Fig. 1 but for the S233 source. In this case, the systemic velocity of the source is −17.2 km s^{-1} (vertical dashed line).

flux density. The peaks of the two spectral features are situated at −17 and −19 km s^{-1}. The most intense maser feature was observed in March, 2001 at V_{LSR} = −17.0 km s^{-1} (∼ 43 Jy), with a velocity similar to that of the AFGL 5157 molecular core (−17.8 km s^{-1}, Torrelles et al. 1992b). However, this feature was not present in May, 1999 (see Fig. 1).

4.2. *S233*

S233 belongs to a small group of H II regions (S231, S233, and S235) located in the Perseus arm at a distance of 1.8 kpc. Following the Hodapp (1994) and Tofani et al. (1995) nomenclature, we will refer to the region where the IRAS 05358+3543 source is located as S233. A CO outflow (Snell, Dickman, & Huang 1990) centered on this IRAS source has been observed. In addition, H_2O masers have been detected in this region without the presence of any continuum radio source (Tofani et al. 1995).

During the five months monitoring of S233 (from March to July 2001), three maser features with velocities of −17.5, −16.3, and −14.1 km s^{-1} were detected (see Figure 2). In the first observing run, two relatively weak features (18 and 30 Jy at V_{LSR} = −16.3 and −17.5, respectively) were detected, but their peak flux density increased with time, reaching their maxima in June 2001 (63 and 157 Jy). In addition, in June 2001 a third feature, relatively weak (23 Jy at V_{LSR} = −14.1), appeared in the spectra, but was absent when observing in July. This behavior is similar to that found by Wootten (1993) in IRAS 16293–2422, where high velocity features tend to be weaker and more transitory than low velocity features.

4.3. *AFGL 5182*

This source is located at a distance of 1.5 kpc. Szymczak, Hrynek, & Kus (2000) have found methanol maser emission in the velocity range from −13 to 0 km s^{-1} around AFGL 5182, coinciding with the velocity of the water maser features observed by Wouterloot, Brand, & Fiegle (1993). Radio continuum emission has also been detected in this region. For instance, Kurtz, Chruchwell, & Wood (1994) observed three sources at 3.6 cm, but none of them seem to coincide with the AFGL 5182 source.

Figure 3 shows that the maser activity in this region is very intense and that in the time interval of our observations its maximum activity occurred in May 2001, when eight features were observed in the spectra. The strongest maser feature was observed in May 1999 (354 Jy), and its peak flux density diminished systematically with time (34 Jy in July 2001). In general, the observed maser features can be divided into two main groups; one of them blueshifted (from −10.6 to −1 km s^{-1}), and the other one redshifted (from 10 to 17 km s^{-1}), with respect to the systemic velocity of the source (−0.7 km s^{-1}). Given

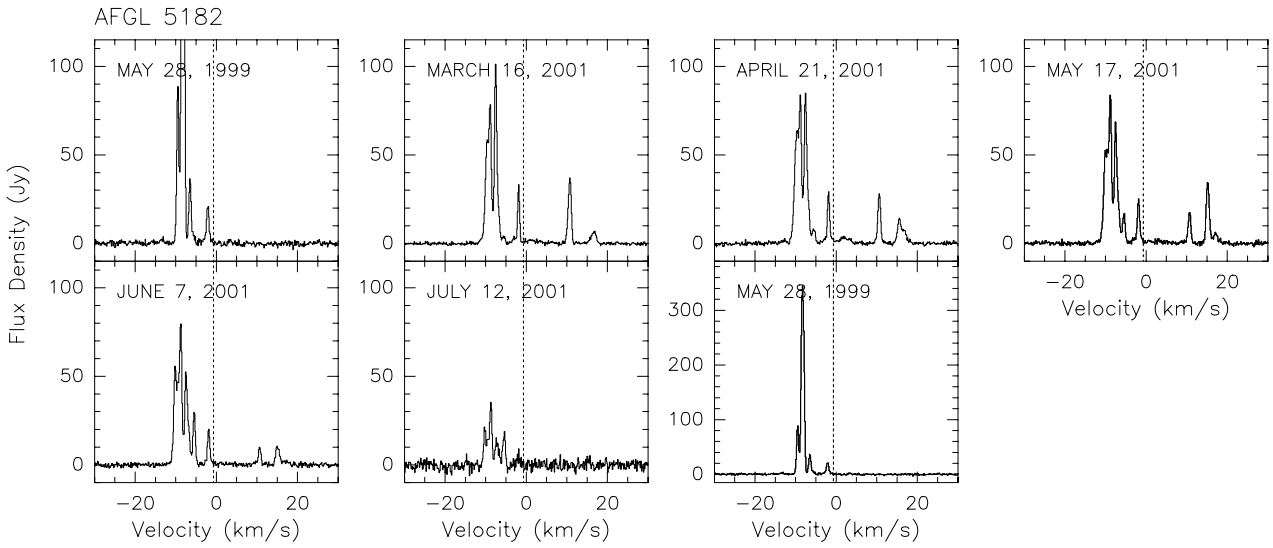

Fig. 3. Same as Fig. 1 but for the AFGL 5182 source. In this case, the systemic velocity of the source is -0.7 km s^{-1} (vertical dashed line). The first spectrum is repeated at the end of the sequence but with a different scale for the peak flux density.

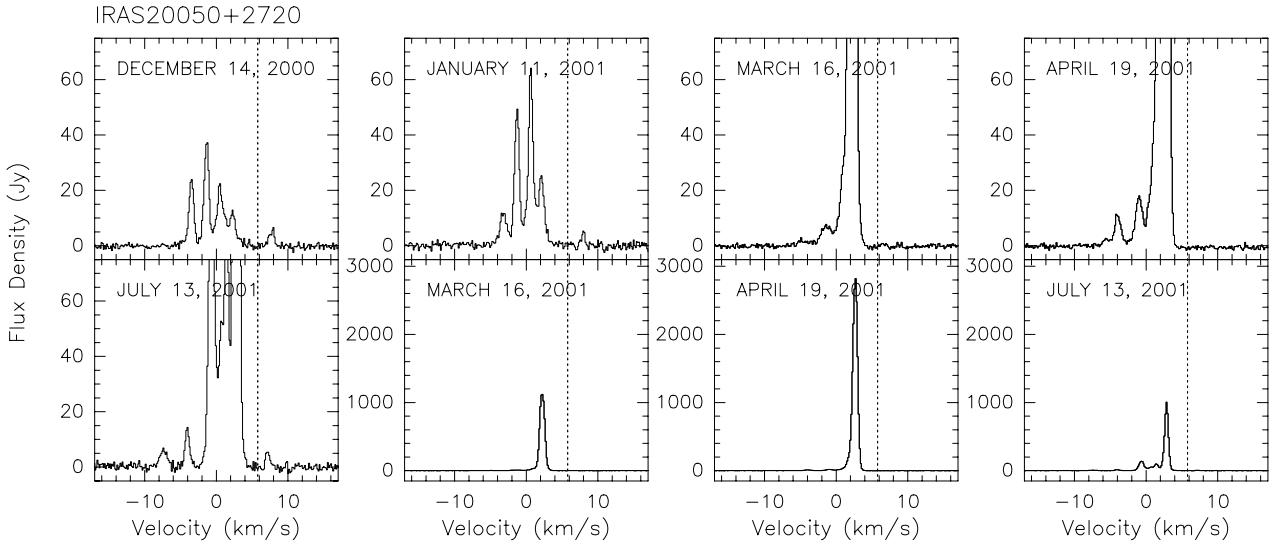

Fig. 4. Same as Fig. 1 but for the IRAS 20050+2720 source. In this case, the systemic velocity of the source is 5.8 km s^{-1} (vertical dashed line). Some spectra are repeated with a different scale for the peak flux density.

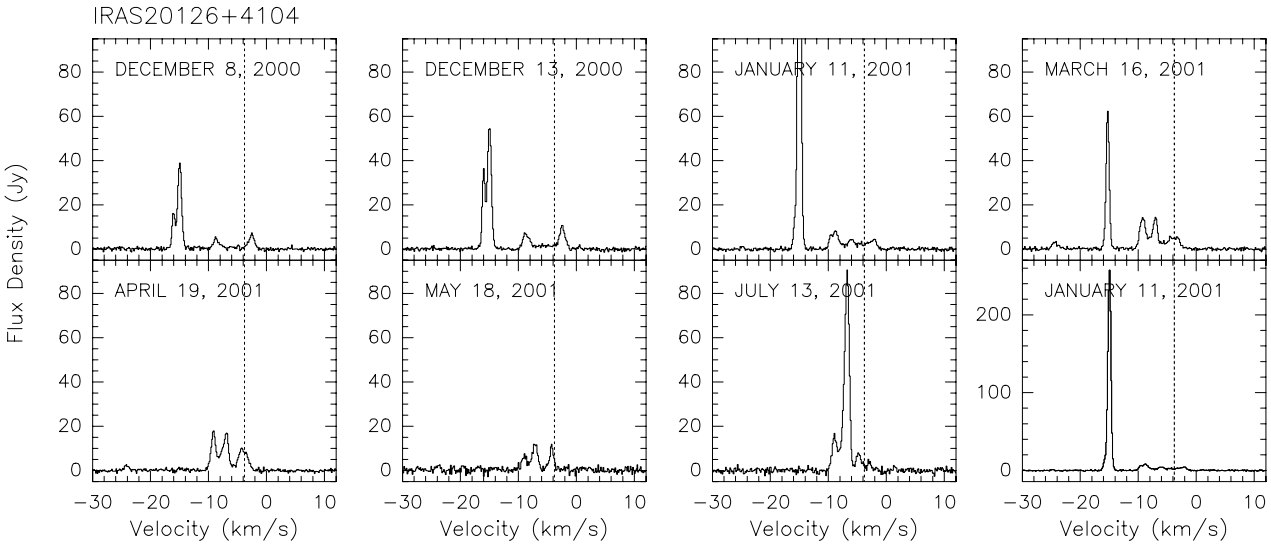

Fig. 5. Same as Fig. 1 but for the IRAS 20126+4104 source. In this case, the systemic velocity of the source is −3.8 km s^{-1} (vertical dashed line).

these kinematic characteristics it is possible that the water maser emission in this source is tracing a bipolar outflow, a suggestion that can be tested with high angular resolution observations.

4.4. *IRAS 20050+2720*

With a luminosity of 260 $L_{\odot}$, this is the weakest source of the sample. It is located in the Cygnus Rift at a distance of 700 pc (Bachiller, Fuente, & Tafalla 1995). Its environment is quite complex; there is a quadrupolar molecular outflow in the region, which is apparently associated with this source. However, observations of Anglada, Rodríguez, & Torrelles (1998) found that there are two radio continuum sources in the region, each of them apparently driving its own outflow.

The spectra show very intense water maser features. In fact, after Cepheus A, this is the source with the strongest maser feature ($\sim$ 2800 Jy) in the sample. The maser features in this region changed drastically in peak flux density between January and April, 2001. In particular, the feature at $V_{LSR} = 2.4$ km s^{-1} changed its peak flux density by more than two orders of magnitude (see Figure 4). Such large variations suggest very intense activity around the IRAS 20050+2720 source. The velocity of the observed water maser features ranges from −8 to 8.2 km s^{-1}, most of them being blueshifted with respect to the systemic velocity of the source (+5.8 km s^{-1}). In our observations we do not detect the extremely high velocity (EHV) water maser feature at $V_{LSR} = -91$ km s^{-1}, nor the intermediate velocity features at $V_{LSR} = -24$ and −36 km s^{-1} observed by Furuya et al. (2001; 2003), which were suggested to be associated with the EHV CO outflow observed in the region (Furuya et al. 2003).

4.5. *IRAS 20126+4104*

The IRAS 20126+4104 source is located in a dark cloud in the Cygnus-X region, at a distance of 1.7 kpc (Wilking et al. 1989). Its luminosity in the far infrared is 1.3×10^4 $L_{\odot}$ (Wood & Churchwell 1989). This source is located near the center of a CO molecular outflow oriented in the north-south direction (Wilking, Blackwell, & Mundy 1990). Observations from near infrared to millimeter wavelengths (Cesaroni et al. 1999) show that IRAS 20126+4104 is an excellent example of a massive proto-star with a Keplerian disk and a bipolar jet/outflow. In addition, Moscadelli, Cesaroni, & Rioja (2000) have found that water masers associated with the IRAS source appear to be located on the surface of a bipolar conical jet.

Figure 5 shows the observed spectra of the IRAS 20126+4104. This source was observed during a period of 216 days, from December 2000 to July 2001, at approximately one-month intervals. The maser features are concentrated in the velocity range from −25.0 to −1 km s^{-1}. During the observations, the source was quite active and the maser emission showed a large variability. The strongest feature was observed in January 2001 (255 Jy, $V_{LSR} = -15.1$ km s^{-1}), although this maser feature became unde-

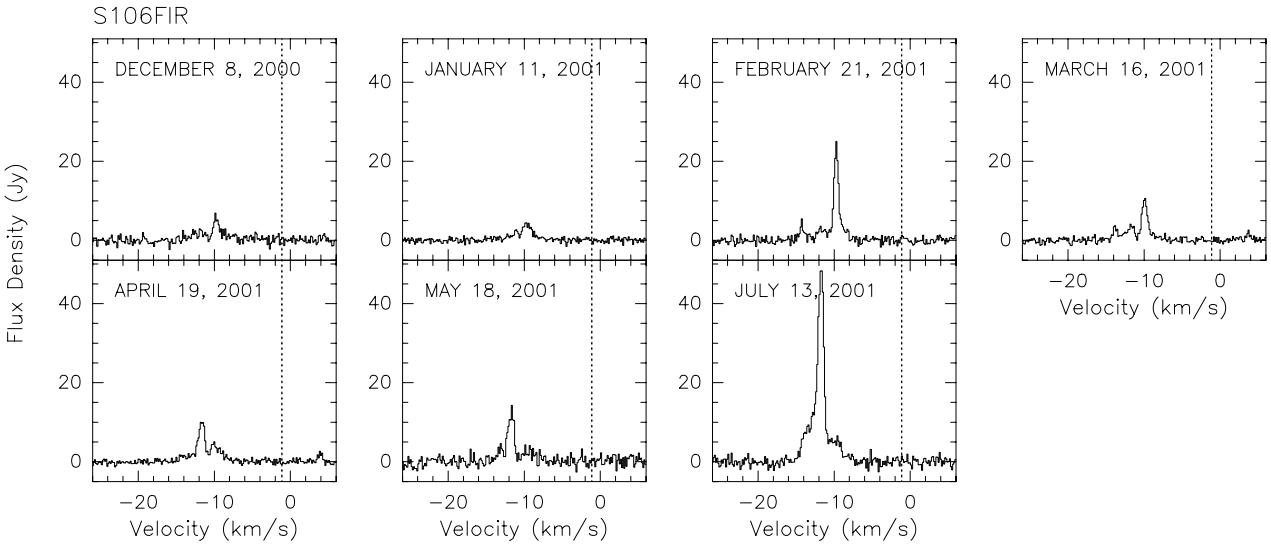

Fig. 6. Same as Fig. 1 but for the S106 FIR source. In this case, the systemic velocity of the source is -1.1 km s^{-1} (vertical dashed line).

tectable in April of the same year and it remained turned off during the rest of the observations. In July 2001, the maser feature at $V_{LSR} = -7.0$ km s^{-1} became the strongest feature in the region. In addition, a very weak feature ($\sim$ 3 Jy at $V_{LSR} = -24$) was observed in March and April. Similar short lifetime, low flux density features have also been observed at intermediate and high velocities in IRAS 16293–2422 (Wootten 1993). Finally, we have not detected any maser feature that would coincide in velocity with the methanol maser feature ($V_{LSR} = -6.1$ km s^{-1}) detected by Szymczak et al. (2000).

4.6. *S106 FIR*

Sharpless 106 (S106) is a darkened bipolar H II region embedded in a molecular cloud (Lucas et al. 1978), and located at a distance of approximately 600 pc (Staude et al. 1982). S106 FIR is a bright source in the far infrared (Richer et al. 1993), and it has been cataloged as a Class 0. This source is located 15″ to the west and 2″ to the south of IRS 4. Observations from Furuya et al. (1999) showed that the water masers detected in the region are associated with a jet-like outflow, quite compact and very collimated, that is accelerating.

In most of our observations (see Figure 6) the S106 FIR source showed weak (of the order of 10 Jy) maser emission, except in July 2001, where the flux density of the maser feature at $V_{LSR} = -11.8$ km s^{-1} reached 46 Jy. The spectra of the source are shown in Fig. 6, where it can be seen that the maser features range in velocity from -14.5 to -9 km s^{-1}. All maser features are blueshifted and the velocity of the strongest feature ($V_{LSR} = -11.8$ km s^{-1}) is very different from the systemic velocity of the cloud (-1.1 km s^{-1}). The redshifted maser feature observed by Furuya et al. (1999;2003) was not detected in our observations. Observing the blueshifted maser feature at $V_{LSR} = -9.8$ km s^{-1} from December 8, 2000 to March 16, 2001, a velocity drift of about 0.2 km s^{-1} was found. This feature seems to have a radial acceleration of about 0.8 km s^{-1} yr^{-1} moving towards us along the line of sight, confirming that maser features in S106 FIR trace an accelerating jet-like outflow. However, the acceleration calculated in this work is somewhat less than that found by Furuya et al. (1999) (1.1 km s^{-1}) in similar time periods (100 days).

4.7. *AFGL 2591*

AFGL 2591 is a star-forming region located at a distance of 1 kpc. In this region a very bright infrared source has been observed (9×10^4 $L_\odot$, Lada et al. 1984), probably associated with the powering source of the molecular outflow observed in the region (Bally & Lada 1983; Torrelles et al. 1983; Mitchell, Maillard, & Hasewaga 1991). In addition, there are three radio continuum sources, two of them spatially coincident with H_2O maser emission (VLA 2 and VLA 3; Trinidad et al. 2003a).

The spectra observed during the monitoring period are shown in Figure 7. The first spectrum was observed in May 1999 and the rest from December 2000 to July 2001, at approximately one-month in-

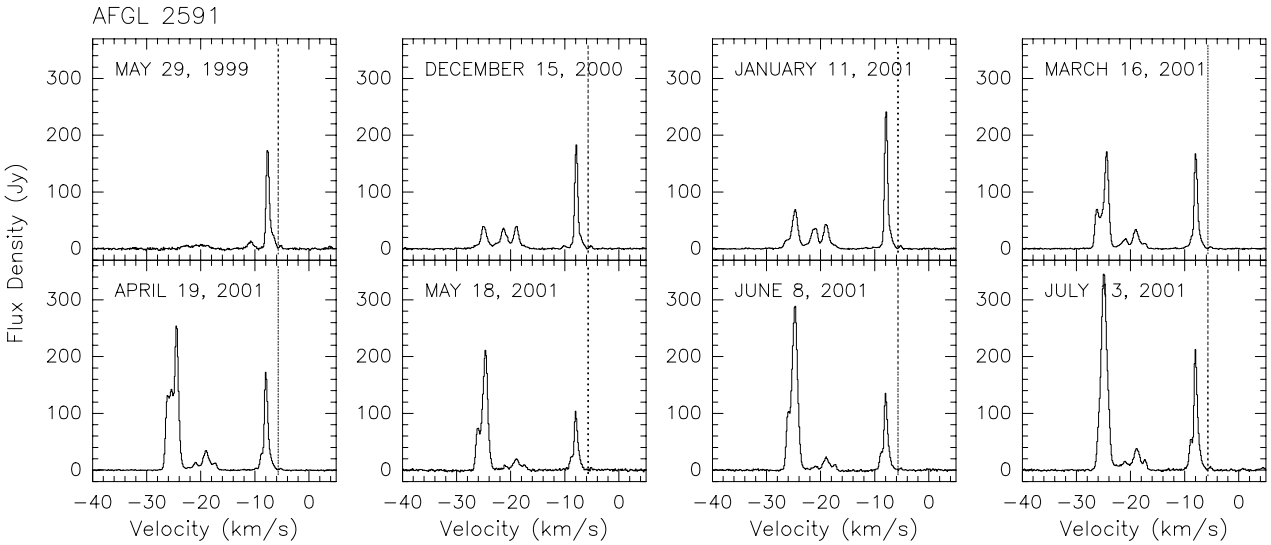

Fig. 7. Same as Fig. 1 but for the AFGL 2591 source. In this case, the systemic velocity of the source is -5.7 km s^{-1} (vertical dashed line).

tervals. This figure shows that the spectra are rich in maser features (six during the maximum activity) and that they range in velocity from -27 to -6 km s^{-1}.

There is a water maser feature at -7.9 km s^{-1}, close to the molecular cloud velocity (~ -7 km s^{-1}), that was present during the whole observing period. This maser feature showed some variability in its peak flux density, but it remained always in the range from 90 to 240 Jy. On the other hand, the maser feature at -24.7 km s^{-1} was the strongest feature, reaching a peak flux density of 330 Jy in July 2001, although in May 1999 this feature practically disappeared (see Fig. 7). This strong, intermediate velocity feature had a very long lifetime (eight months) compared with other features with similar velocities. In general, all water maser features in this source showed variations in their peak flux density from one observation to the next.

4.8. *LkHα 234*

LkHα 234 is a Herbig Be star of intermediate luminosity (1.3×10^3 $L_\odot$, Bechis et al. 1978) located in the NGC 7129 region. Two H_2O masers were detected by Rodríguez & Cantó (1983) in this region. Using these data, Rodríguez et al. (1987) concluded that this type of stars (of intermediate luminosity) are able to produce water maser activity at relatively large distances ($\geq 10^{16}$ cm).

The water maser emission associated with LkHα 234 was quite active during the whole period of its monitoring (see Figure 8). The first observations were carried out in June 1999 and after that, from December 2000 to July 2001, at approximately one-month intervals providing nine spectra of this region. A total of eight spectral features were observed in the velocity range from -25 to -5 km s^{-1}; however, we did not detect the maser features at $V_{LSR} = -40.7$ and 2.4 km s^{-1} observed by Furuya et al. (2003).

The strongest maser feature was detected in December 2000 ($\sim$ 100 Jy) at $V_{LSR} = -9$ km s^{-1}, close to the molecular cloud velocity ($V_{LSR} = -10$ km s^{-1}). This feature was always detected in our observations, although its peak flux density decreased with time, reaching $\sim$ 45 Jy in July 2001. Another maser feature that was present during all the observations is the one at $V_{LSR} = -17.5$ km s^{-1}, but it was not so intense as the one at -9 km s^{-1}. Its maximum ($\sim$ 70 Jy) was observed in June 1999, then its peak flux density decreased considerably ($\sim$ 7 Jy in December 2000), and it continued almost constant during the rest of the observations. In general, the observed maser features can be divided into two main groups; one of them redshifted (from -5 to -9.5 km s^{-1}), and the other one blueshifted (from -13 to -25 km s^{-1}) with respect to the systemic velocity of the source (-10 km s^{-1}). This result suggests that the water maser emission in this source traces a bipolar outflow, as has recently been showen by Trinidad et al. (2003b), using high angular resolution observations.

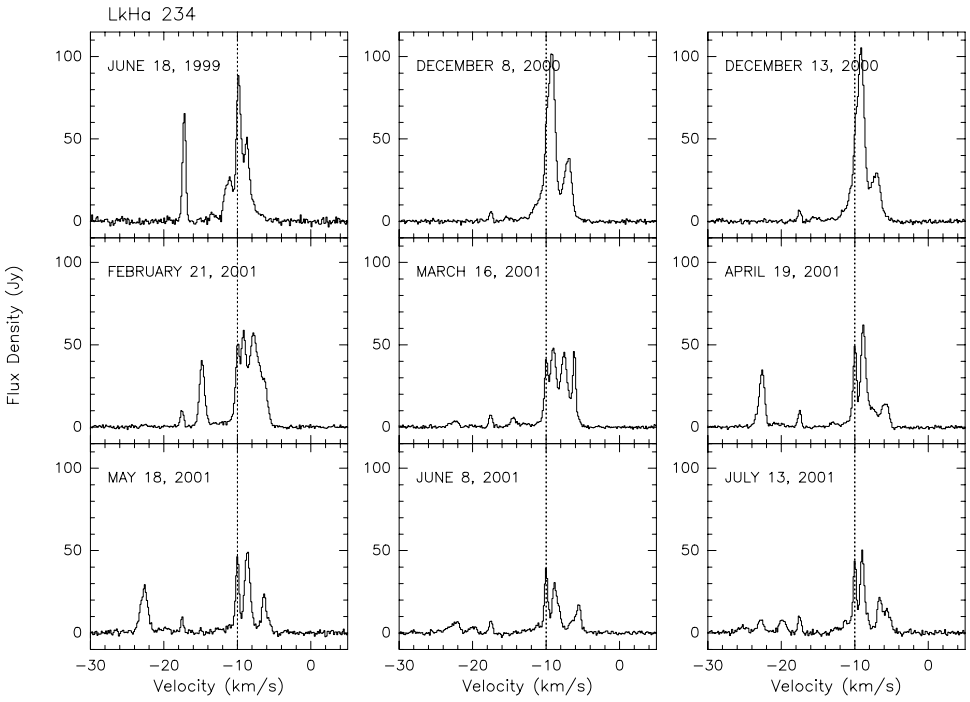

Fig. 8. Same as Fig. 1 but for the LkHα 234 source. In this case, the systemic velocity of the source is -10.0 km s^{-1} (vertical dashed line).

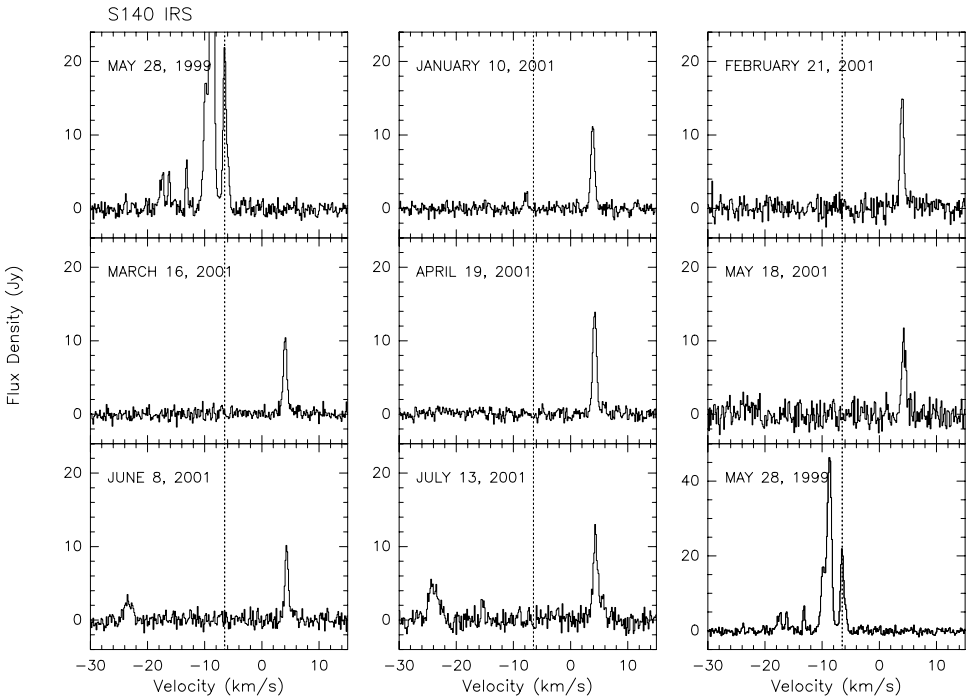

Fig. 9. Same as Fig. 1 but for the S140 IRS source. In this case, the systemic velocity of the source is -6.5 km s^{-1} (vertical dashed line). The first spectrum is repeated at the end of the sequence with a different scale for the peak flux density.

4.9. *S140 IRS*

S140 IRS is located in the molecular cloud L1204, at a distance of 910 pc (Crampton & Fisher 1974). In this region there are three infrared sources, IRS1, IRS2, and IRS3 (Beichman, Becklin, & Wynn-Williams 1979), that have radio continuum counterparts (Schwartz 1989). Among the three sources, IRS 1 is the brightest one at both infrared and radio continuum wavelengths.

This region has been extensively studied by Lekht et al. (1993) and Lekht & Sorochenko (2001). They have observed water masers during 18 years (from 1981 to 1999) with a single antenna. They obtained a spectrum of three maser features; the central component has a velocity close to that of the molecular cloud, and the lateral ones are redshifted and blueshifted, respectively. The anticorrelation observed between the central feature and the lateral ones was interpreted as a Keplerian disk in S140 IRS. On the other hand, Valdettaro et al. (2002) have observed water masers in this region from 1987 to 1999 with the 32 m Medicina antenna , but they did not confirm the results found by Lekht et al. (1993) and Lekht & Sorochenko (2001).

Our observations of the water masers in S140 IRS were carried out in May 1999 and from January to May 2001. The maximum activity was registered during the first observations, showing six spectral features. The strongest feature was detected at $V_{LSR} = -8.7$ km s^{-1} with a peak flux density of ~ 50 Jy (see Figure 9). When we observed it again in January 2001, its maser activity had diminished considerably and practically all features detected in May 1999 had disappeared. A new and single weak maser feature was detected in January 2001 and remained practically the only feature in the spectrum until June 2001 when a weak new feature appeared.

4.10. *CEPHEUS A*

Cepheus A is a star-forming region located at a distance of 730 pc (Johnson 1957). HW2 is probably the exciting source of the energetic molecular outflow observed in this region (Hughes & Wouterloot 1984), which is one of the best examples of outflows associated with a high-mass protostar. Maser emission of OH and H_2O has been observed toward the Cepheus A region. The OH masers seem to be located in an expanding structure that may be tracing a shell (Cohen, Rowland, & Blair 1984; Migenes, Cohen, & Brebner 1992) and H_2O seems to be tracing a circumstellar disk (e.g., Torrelles et al. 1996) around HW2.

The Cepheus A maser spectra are shown in Figure 10. This source was observed in May and June 1999, and then from December 2000 to July 2001, at approximately one-month intervals. The strongest maser feature ($V_{LSR} = -9.7$ km s^{-1}) in Cepheus was used to calibrate the telescope pointing; therefore, this source was observed several times, at least twice during each observing epoch. Fig. 10 shows that the maser activity in Cepheus A is very intense, containing the strongest feature in the whole sample ($\sim$ 7350 Jy). The detected maser features are concentrated in the velocity range from -24 to -2 km s^{-1}.

Some maser features observed in May and June 1999 were not detected during the observations from December 2000 to July 2001. Three maser features, at $V_{LSR} = -8.9$, -9.7, and, -14.3 km s^{-1}, were observed during all the epochs, reaching a maximum peak flux density of ~ 1000, ~ 7350 and ~ 850 Jy, respectively.

4.11. *IRAS 23139+5939*

This source, with a luminosity of $1.9 \times 10^4 L_\odot$, is one of the farthest of our sample (3.5 kpc) and is located near S157. CO observations show that there is intense emission associated with IRAS 23139+5939 at a velocity of -44 km s^{-1}, suggesting the presence of a molecular outflow (Wouterloot, Henkel, & Walmsley 1989). In addition, Tofani et al. (1995) have detected a weak radio continuum source (0.6 mJy) at 8.4 GHz and H_2O maser emission associated with this source.

The IRAS 23139+5939 source was observed for the first time in May 1999. We obtained seven spectra, taken about one month apart (except January) from December 2000 to July, 2001.

The observed maser features range in velocity from -54.5 to -42.5 km s^{-1}, the feature at $V_{LSR} = -52.5$ km s^{-1} being the strongest during all the observations. This velocity range is completely different from that of the methanol masers observed by Szymczak et al. (2000), which range in velocity from -42 to -37 km s^{-1}.

Figure 11 shows that the water maser spectrum associated with this source has a three-peak structure, similar to that found in S255 (Cesaroni 1990) and S140 IRS (Lekht et al. 1993), where this feature has been interpreted, based on its variability and anticorrelation of their features, as being associated with a Keplerian disk seen edge-on. However, the water masers observed around IRAS 23139+5939 are probably not associated with a Keplerian disk, since in this model the velocity of the central maser feature is expected to be similar to the molecular cloud velocity, and the lateral maser features shoul

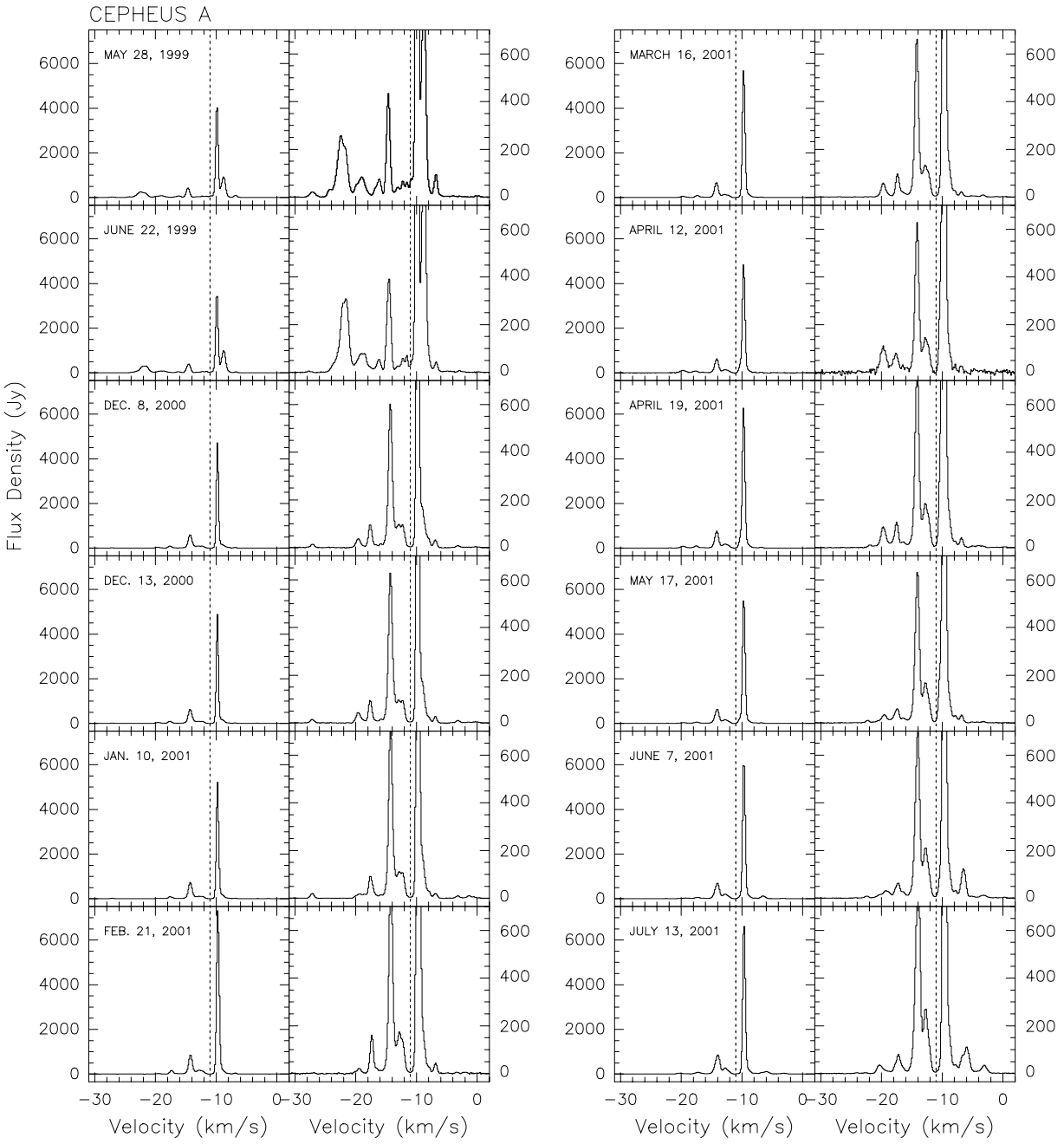

Fig. 10. Same as Fig. 1 but for the Cepheus A source. In this case, the systemic velocity of the source is -11.0 km s^{-1} (vertical dashed line). Each spectrum is shown at two different scales to better appreciate the dynamic range of the maser features.

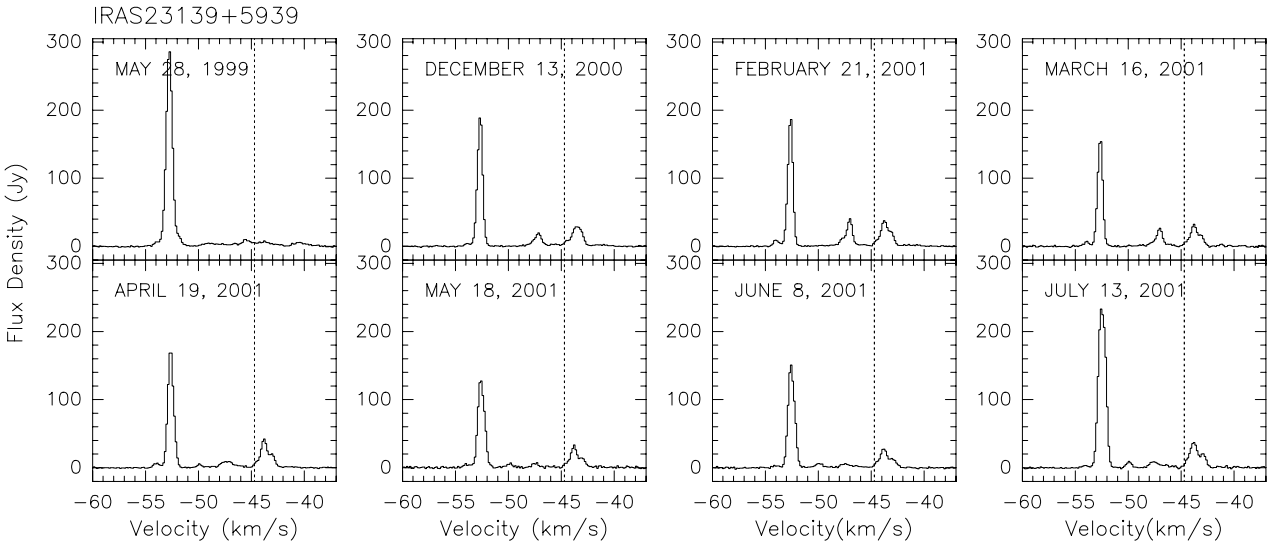

Fig. 11. Same as Fig. 1 but for the IRAS 23139+5939 source. In this case, the systemic velocity of the source is −44.7 km s^{-1} (vertical dashed line).

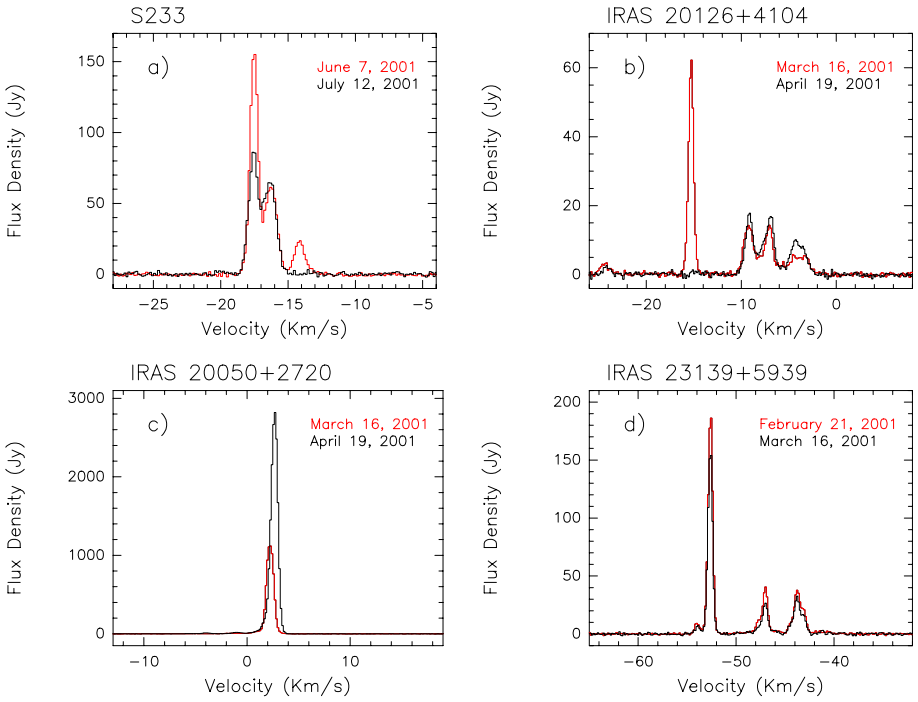

Fig. 12. Maser variability of four selected YSOs. This figure shows four different kinds of maser variability found in the sample (see subsection 5.1). The two spectra in each panel were taken about one month apart. The first observed spectrum is shown in gray and the second is shown in black.

be redshifted and blueshifted. In IRAS 23139+5939, the maser feature with the velocity closest to that of the molecular cloud (-44 km s^{-1}) is one of the lateral features, and the other two are blueshifted.

5. DISCUSSION

5.1. *Variability*

From our observations of water masers, we have found different kinds of maser variability in the observed sample of YSOs. The variability of the maser features can be divided in four main groups (see Figure 12) according to their behavior during the observations: a) the weakest component disappears (or appears), b) the strongest maser feature disappears (or appears), c) the maser features change their peak flux density by more than a factor of two, and, d) the maser features show small variations.

The spectra discussed in the previous section show that all the observed sources have maser features, whose peak flux densities change with time in scales ranging from one month (or less) up to several months. Then, in order to find a periodicity pattern in the variability of the water masers, we have selected the maser features of each source that were present in at least half of the observed spectra. Figure 13 shows the peak flux density of the selected maser features of each source as a function of time. We can qualitatively determine the tendency of the variability in the sample of the H_2O masers. We find that in all sources at least one maser feature appeared or disappeared during the observations, and that in about half of the sources at least one maser feature increased systematically its peak flux density with time. However, based on the data that we present here, it is not possible to determine if any of the maser features has a periodicity pattern. Furthermore, we do not find any relationship between the luminosity of the sources and the variability of the water maser features.

So far, we have only analyzed the variability of the water masers in a qualitative way. Then, in order to quantify the degree of variability of the maser features, we can estimate the variability index of all the maser features in the selected sample. The variability index is defined as $V_i = F_{max}/F_{min}$ (Palagi et al. 1993; Persi et al. 1994), where F_{max} and F_{min} are the maximum and minimum observed peak flux density for each maser feature during the monitoring period. In those cases where a maser feature appears or disappears, a lower limit for the variability index can be obtained by taking F_{min} as the value of the noise level in the spectrum. The estimated values of the variability index (including lower limits) of all maser features are listed in Table 2, and their distribution is shown in Figure 14. From the variability indices, we find that all the sources have maser features with $V_i < 10$ and that about 60% of the sources have at least a maser feature that shows large variations in the peak flux density ($V_i > 10$). Although Fig. 14 does not provide information about any source in particular, it does show the tendency of the water maser variability of the sources as a whole. The histogram shows that about half of the maser features have variability indices between one and four, although a wide range of values is found.

We have tried to provide a statistical description to the results shown in Fig. 14 as follows. We first assume that the intensity of the masers, I, is given by an exponential amplification:

$$I = I_0 \; exp(+\tau),$$

where τ is the absolute value of the opacity of the feature at a given time. We now adopt a Gaussian (normal) probability distribution for that opacity:

$$p(\tau) = \frac{1}{(2\pi\sigma^2)^{1/2}} \; exp[-(\tau_0 - \tau)^2/2\sigma^2],$$

where τ_0 is the mean opacity and σ is the standard deviation of the opacity. The probability distribution for the opacity ratio of independent observations of the same feature has a standard deviation equal to $2^{1/2}\sigma$ and will then be given by:

$$O(\delta\tau) = \frac{1}{(4\pi\sigma^2)^{1/2}} \; exp[-(\delta\tau)^2/4\sigma^2].$$

In the above equation $\delta\tau$ is the difference in opacity between the two observations. We now make the assumption that all masers observed have the same σ. Then, following Maisel (1971), the probability distribution for the variability index, V, will be given by:

$$p(V) = \frac{1}{(\pi\sigma^2)^{1/2}V} \; exp[-(ln\ V)^2/4\sigma^2], \qquad (1)$$

with $p(V) = 0$ for $V < 1$. We note that this probability distribution depends only on the value of σ.

To have more data, we have added to our table of variability indices those obtained by Persi et al. (1994), reaching a total of 84 maser features. Using the equation given above with $\sigma = 1.6$, we obtain a reasonable fit to the data, as shown in Figure 15. Larger or smaller values of σ provide a poorer fit. The acceptable fit obtained suggests that the water

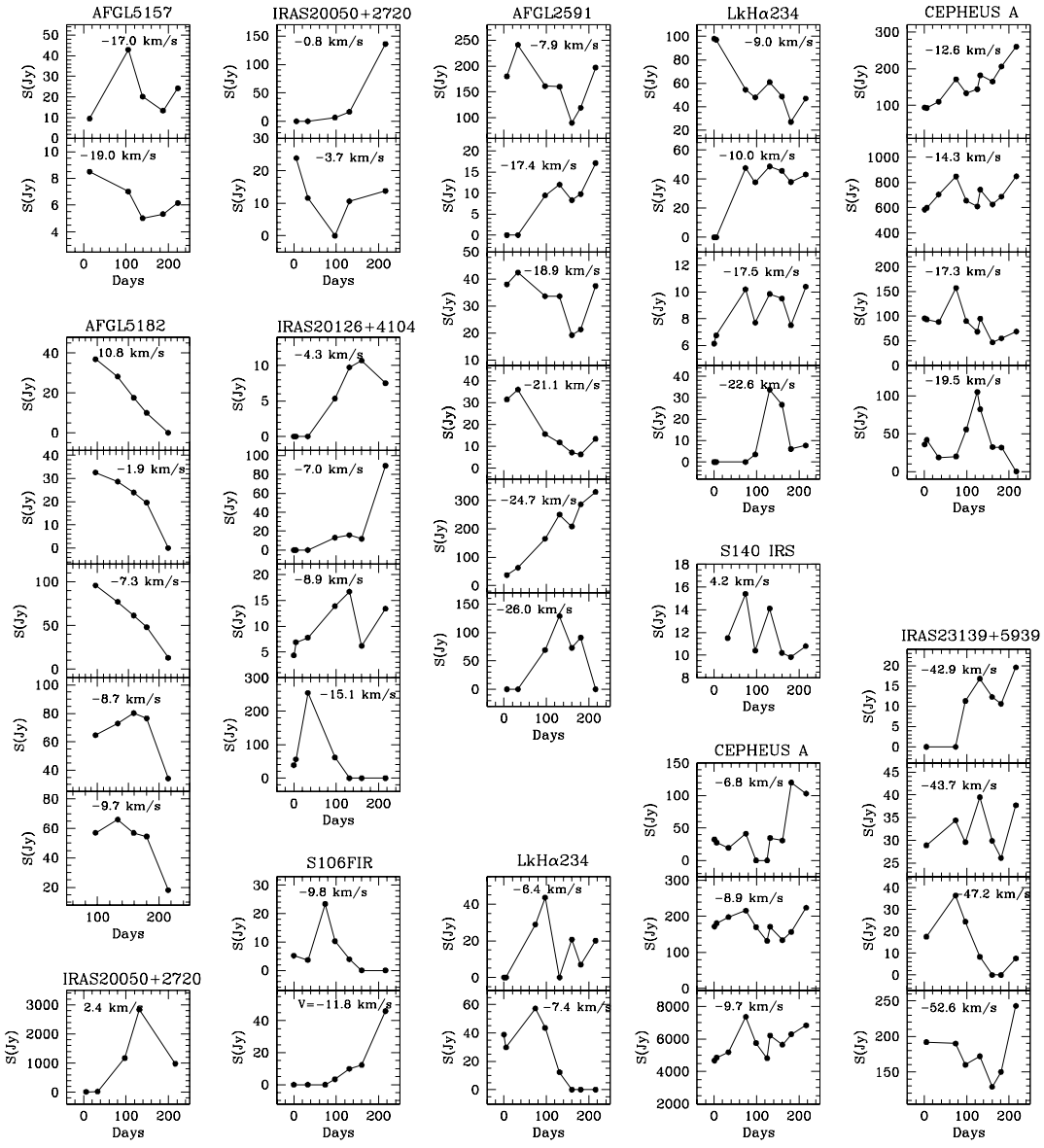

Fig. 13. Temporal variations of the peak flux density of several maser features of the observed sources. The maser features were selected such that they were present in at least half of the spectra obtained for each observed source.

TABLE 2

PARAMETERS OF THE WATER MASER FEATURES

Source	Velocity Range		F_{peak}	V_{LSR}	V_i	Variability	CO Outflow	
	V_{min}(km/s)	V_{max}(km/s)	(Jy)	(km s^{-1})		Rate	V_{blue}(km/s)	V_{red}(km/s)
AFGL5157	-23.0	–13.0	42.9	–17.0	4.5	1.5	–30.0	–3.0
			8.5	–19.0	1.7	0.4		
S233	–18.0	–13.7	23.0	–14.1	$\geq$ 2.7	$\geq$ 4.1	–32.0	–4.0
			66.4	–16.3	3.7	1.0		
			157.0	–17.5	5.0	1.8		
AFGL5182	–10.6	17.0	7.2	16.7	$\geq$ 1.7	$\geq$ 2.0	....	....
			34.8	15.3	$\geq$ 10.9	$\geq$ 5.3		
			36.9	10.7	3.7	1.3		
			32.6	–1.9	$\geq$ 2.6	$\geq$ 0.7		
			29.5	–5.5	$\geq$ 7.8	$\geq$ 5.0		
			95.8	–7.3	7.4	1.9		
			80.2	–8.7	2.4	1.3		
			66.0	–9.7	3.7	1.4		
IRAS20050+2720	–8.0	8.2	5.5	7.8	$\geq$ 1.7	$\geq$ 0.6	–70.0	70.0
			2842.0	2.4	256.0	61.4		
			79.1	1.4	$\geq$ 24.7	$\geq$ 8.7		
			61.5	0.6	$\geq$ 19.2	$\geq$ 9.0		
			136.0	–0.8	$\geq$ 25.7	$\geq$ 4.2		
			48.1	–1.3	$\geq$ 15.0	$\geq$ 7.1		
			23.9	–3.7	$\geq$ 7.5	$\geq$ 2.5		
IRAS20126+4104	–25.0	–1.0	34.3	–2.5	$\geq$ 3.4	$\geq$ 1.1	–41.9	34.9
			10.7	–4.3	$\geq$ 3.3	$\geq$ 0.8		
			89.1	–7-.0	$\geq$ 27.8	$\geq$ 4.6		
			16.7	–8.9	3.8	0.9		
			255.0	–15.1	$\geq$ 85.0	$\geq$ 26.0		
			34.3	–15.9	$\geq$ 10.7	$\geq$ 11.5		
S106FIR	–14.5	–9.0	23.4	–9.8	$\geq$ 2.8	$\geq$ 0.6	....	....
			46.0	–11.8	$\geq$ 13.6	$\geq$ 3.4		
AFGL2591	–27.0	–6.0	241.0	–7.9	2.7	0.6	–21.9	14.5
			17.1	–17.4	$\geq$ 4.1	$\geq$ 0.7		
			42.4	–18.9	2.2	0.5		
			36.0	–21.1	5.7	1.2		
			330.0	–24.7	8.9	1.3		
			129.0	–26.0	$\geq$ 23.3	$\geq$ 8.2		
LkHα234	–25.0	–5.0	16.1	–5.6	$\geq$ 2.3	$\geq$ 3.3	–14.1	18.7
			43.6	–6.4	$\geq$ 13.6	$\geq$ 12.0		
			57.2	–7.4	$\geq$ 8.1	$\geq$ 2.8		
			98.1	–9.0	3.6	0.7		
			48.7	–10.0	$\geq$ 9.2	$\geq$ 2.8		
			39.5	–14.8	$\geq$ 9.4	$\geq$ 12.3		
			10.4	–17.5	1.7	0.3		
			8.1	–19.9	$\geq$ 2.8	$\geq$ 1.9		
			33.7	–22.6	9.6	8.5		
S140IRS	–25.0	5.0	15.4	4.2	1.6	0.4	–24.0	6.0
			4.6	–23.9	$\geq$ 1.8	$\geq$ 1.5		

TABLE 2 (CONTINUED)

Source	Velocity Range		F_{peak}	V_{LSR}	V_i	Variability	CO Outflow	
	V_{min}(km/s)	V_{max}(km/s)	(Jy)	(km s^{-1})		Rate	V_{blue}(km/s)	V_{red}(km/s)
CEPHEUS A	–24.0	–2.0	120.0	–6.8	17.4	5.6	–25.0	5.0
			1007.0	–8.9	1.7	0.6		
			7368.0	–9.7	1.6	0.7		
			260.0	–12.6	2.8	0.4		
			849.0	–14.3	1.5	0.2		
			157.0	–17.3	3.4	1.2		
			105.0	–19.5	5.8	1.9		
IRAS23139+5939	–54.5	-4-2.5	19.6	–42.9	≥ 6.1	≥ 1.3	–59.0	–31.0
			39.5	–43.7	1.5	0.9		
			36.4	–47.2	≥ 5.2	≥ 1.8		
			8.21	–50.0	≥ 2.0	≥ 1.7		
			243.0	–52.6	1.9	1.0		
			11.4	–54.0	≥ 2.7	≥ 3.5		

maser variability can be described statistically as due to Gaussian variations in the line opacity.

We then conclude that over the time scales during which the variability indices were obtained, the opacities have a standard deviation of order 1.6. Since the mean opacities of water masers are of order 20 (Reid & Moran 1981), we conclude that variations of order of 10, observed in the intensities of the masers, are the result of small variations of order of 10% in the opacities.

The variability index is calculated using the observed maximum and minimum peak flux densities, and it indicates how much the peak flux density of a given maser feature changes during the observations. However, as Fig. 13 shows, the interval of time between the observed F_{max} and F_{min} is different for each maser feature and thus V_i does not take into account the span of time of the observed variations. In order to try to quantify the activity of the observed water masers, we define the variability rate of a maser feature as $VR = V_i/(\Delta t/\delta t)$, where V_i is the variability index, Δt is the interval of time between the F_{max} and F_{min} of the maser feature and δt is an interval of time that characterizes the observations. We have chosen δt to be 30 days, the approximate span of time between successive observations. In column 7 of Table 2 we list the variability rate, which is also illustrated in Figure 16, where we note that about 60% of the maser features of the sample increased/decreased its peak flux density by less than a factor of two in a time span of 30 days. The other 40% of the maser features present variability rates higher that 2, and in a few extreme maser features the peak flux density changes by more than an order of magnitude in time span of 30 days. It is important to note that Fig. 16 shows the variability rate of the water maser features in our sample but does not give information about a specific source.

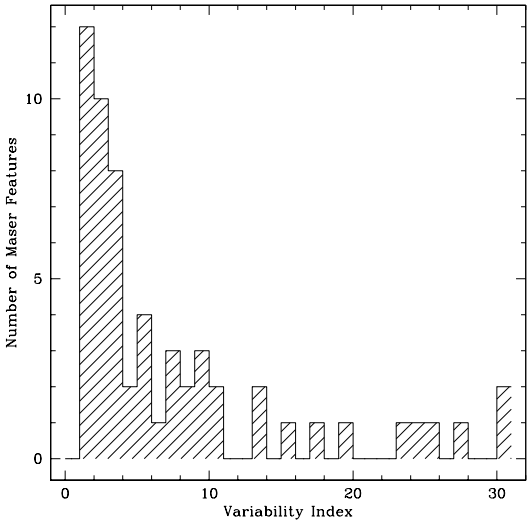

Fig. 14. Distribution of the estimated variability index for all the maser features of the sample of YSOs. Lower limits for the variability index are also included. The horizontal axis is the variability index ($V_i = F_{max}/F_{min}$) and the vertical axis is the number of maser features. The histogram does not give any information about any source in particular, it only shows the tendency of the variability of all the sources in the sample. The last bin includes values greater than 30.

On the other hand, six of our sources were observed with high angular resolution with the VLBA

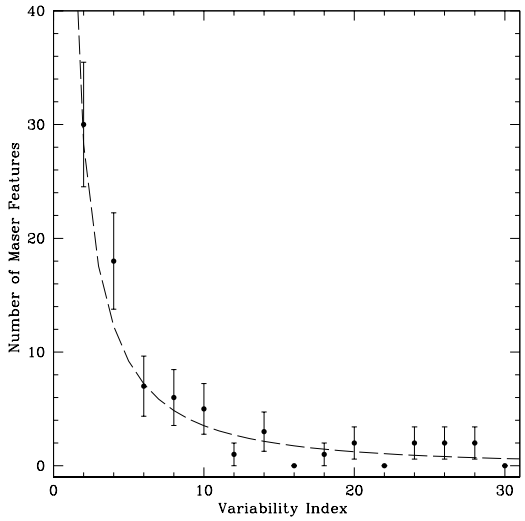

Fig. 15. Distribution of the variability index in the sample obtained from combining the results of Persi et al. (1994) and this paper. The data have been distributed in bins of width 2. The dashed line is the fit using equation 1.

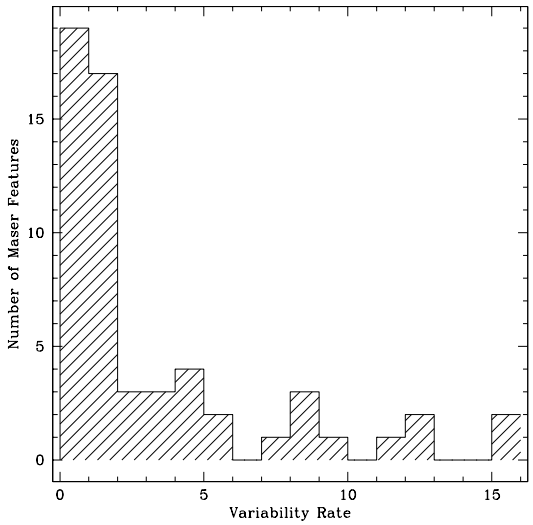

Fig. 16. Distribution of the variability rate of all maser features observed in the sample of YSOs. The horizontal axis is the variability rate ($VR = V_i/(\Delta t/\delta t)$) and the vertical axis is the number of maser components. The last bin includes values greater than 15.

by Migenes et al. (1999). The high angular resolution spectra only detected the more compact maser spots. When comparing these spectra with our own low angular resolution ones,, we identified common maser features in both. We find that the common features have a tendency to show high variability in the peak flux density, indicating that compact maser spots are very active. This is expected from the theory of maser emission, since for unsaturated masers the apparent size is inversely proportional to the square root of the gain coefficient. A more detailed and systematic high resolution study, in combination with single-dish observations, is needed to truly understand the variability of the maser emission.

In Table 2 (column 8 and 9) we list the velocity range of the 9 CO molecular outflows observed in the 11 studied regions. We find that in seven of the sources, the velocity of the maser features lies within the velocity range of the CO outflow (in 2 cases $V_{H_2O} \ll V_{CO}$, in 3 cases $V_{H_2O}/V_{CO} \sim 0.5$, and in 2 cases $V_{H_2O} \sim V_{CO}$), while in two sources the spectrum shows maser features at velocities higher than those of the CO blue lobes (see Table 2). In addition, we find that in the cases of S233 and IRAS20126+4104, one of the high-velocity maser features has a considerably shorter lifetime than the low velocity features. A similar result was found by Wootten (1993) in IRAS 16292–2422. One might speculate that the higher velocity (and probably more variable) maser features could be part of the molecular outflows, while the lower velocity (and longer lifetime) features are associated rather with compact structures, such as circumstellar disks (e.g., Seth et al. [2002]). However, single-dish observations do not give information about the spatial distribution of the masers, and thus interferometric multi-epoch, high angular observations would be needed to investigate this possibility.

Finally, the present study is based on systematic observations of water masers in a sample of YSOs. With such a study of maser variability it is possible to obtain qualitative information about the maser emission of the observed sources. In addition, statistical properties, such as variability index and variability rate of the water maser features, can also be obtained. However, this statistical information has to be viewed with care, because the period of monitoring of the sources is short and improvement in the signal-to-noise ratio of the maser features can be achieved with new observations, which could give values of the variability index greater than the values obtained in this work. Longer monitoring programs of sources with water maser emission and a larger sample of YSOs will be necessary to study in more detail the evolution of the individual maser features.

TABLE 3

VELOCITY SHIFTS OF THE MASER EMISSION

Source	V_{H_2O}	$V_{H_2O} - V_{cloud}$
AFGL5157	–17.3	0.5
S233	–16.9	0.3
AFGL5182	–3.2	–2.5
IRAS20050+2720	2.1	–3.7
IRAS20126+4104	–12.0	–8.2
S106FIR	–11.1	–10.0
AFGL2591	–19.2	–13.5
LkHα234	–10.8	–0.8
S140IRS	–2.3	4.2
CEPHEUS	–10.3	–0.6
IRAS23139+5939	–50.5	–5.8

5.2. *A Search for Systematic Shifts between the Maser Velocity and the Molecular Cloud Velocity*

In most of the spectra presented in § 4, the H_2O maser emission shows a tendency to be blueshifted with respect to the molecular cloud velocity. In order to investigate this issue, we calculated the velocity shift ($V_{H_2O} - V_{cloud}$) between the intensity-weighted mean radial velocity (V_{H_2O}) of the maser features of each source and that of the associated molecular cloud (V_{cloud}). V_{H_2O} is calculated as $\sum F_i V_i / \sum F_i$, where F_i and V_i are the peak flux density and the radial velocity of the *i-th* maser feature, respectively. Results are listed in Table 3, which contains: source name (column 1), V_{H_2O} (column 2), and velocity shift (column 3).

If sources with small velocity shifts $\leq |0.8|$ km s^{-1} (the estimated random velocities in a region of star formation) are excluded we note that the maser emission in seven sources of the sample tends to be blueshifted with respect to the associated molecular cloud velocity, while only one source is redshifted (S140 IRS). To verify this trend seen in the sources in our sample, we included 61 other sources from the literature (Rodríguez et al. 1980; Felli, Palagi, Tofani 1992, Persi et al. 1994; Miralles, Rodríguez, & Scalise 1994; Valdettaro et al. 2001). Then, from a sample of 69 sources (including the sources in our sample), we find that the maser emission of 34 sources (about one half of the sample) is mainly blueshifted with respect to the associated molecular cloud velocity, and that the maser emission of the remaining sources (35) is mainly redshifted. This result shows that the trend found in our sample is not confirmed by a bigger sample, and that the observed trend could be produced by selection effects.

6. CONCLUSIONS

We have monitored the water maser emission in a sample of eleven embedded sources in star-forming regions with the 37 m Haystack antenna. From the analysis of the maser variability, the main results of the present study are:

1. All the observed YSOs show variations of the water maser emission on time scales of one month or less.

2. All the sources have more than one feature that shows variations in its peak flux density by less than a factor of 10 in time spans of one to several months.

3. About 60% of the sources have at least one feature that shows variations in its peak flux density by more than an order of magnitude in time spans of one to several months. Statistically, the variations in the maser intensity can be described as due to small Gaussian fluctuations in the line opacity. For example, variations of an order of magnitude (or less) could be the result of variations in the opacity of about 10% (or less).

4. The estimated value for the variability rate ($VR = V_i/(\Delta t/\delta t)$) is less than two for 60% of the maser features, although there is a wide range of values.

5. We do not find a relationship between the luminosity of the sources and the variability of the H_2O masers, nor a periodicity pattern in the maser variability in any of the observed sources.

6. We find that in our sample of sources the maser emission shows a tendency to be blueshifted with respect to the associated molecular cloud velocity. However this trend is not confirmed when we include other sources from the literature.

MAT acknowledges the support of DGAPA, UNAM, and of CONACyT (México). SC acknowledges support from CONACyT grant 33933-E. We would like to thank P. Pratap for the allocation of the observing time at Haystack, and P. Shute for his excellent assistance during the observations. We are also grateful to V. Migenes, J. Cantó, and V. Strelnitski for enlightening discussions that helped to improve the present paper.

REFERENCES

Anglada, G., Rodríguez, L. F., & Torrelles, J. M. 1998, in ASP Conf. Ser. Vol. 132, Star Formation with the

Infrared Space Observatory, eds. J. Yun & R. Liseau (San Francisco: ASP), 303
Bachiller, R., Fuente, A., & Tafalla, M. 1995, ApJ, 445, L51
Bally J., & Lada C. J. 1983, ApJ, 265, 824
Bechis, K. P., Harvey, P. M., Campbell, M. F., & Hoffmann, W. F. 1978, ApJ, 226, 439
Beichman, C. A., Becklin, E. E., & Wynn-Williams, C. G. 1979, ApJ, 232, L47
Cesaroni, R. 1990, A&A, 233, 513
Cesaroni, R., Felli, M., Jenness, T., Neri, R., Olmi, L., Robberto, M., Testi, L., & Walmsley, C. M. 1999, A&A, 345, 949
Claussen, M. J., Marvel, K. B., Wootten, A., & Wilking, B. A. 1998, ApJ, 507, L79
Cohen, R. J., Rowland, P. R., & Blair, M. M. 1984, MNRAS, 210, 425
Crampton, D., & Fisher, W. A. 1974, Pub. Dom. Ap. Obs., 14, 12
Felli, M., Palagi, F., & Tofani, G. 1992, A&A, 255, 293
Furuya, R. S., Kitamura, Y., Saito, M., Kawabe, R., & Wootten, H. A. 1999, ApJ, 525, 821
Furuya, R. S., Kitamura, Y., Wootten, H. A., Claussen, M. J., Saito, M., Marvel, K. B., & Kawabe, R. 2000, ApJ, 542, L135
Furuya, R. S., Kitamura, Y., Wootten, H. A., Claussen, M. J., and Kawabe, R. 2001, ApJ, 599, 143L
Furuya, R. S., Kitamura, Y., Wootten, H. A., Claussen, M. J., & Kawabe, R. 2003, ApJS, 144, 71
Hodapp, K. W. 1994, ApJS, 94, 615
Hughes, V. A. & Wouterloot, J. G. A., 1984, ApJ, 276, 204
Imai, H., Deguchi, S., & Sasao, T. 2002, ApJ, 567, 971
Johnson, H. L. 1957, ApJ, 126, 121
Kurtz, S., Churchwell, E., & Wood, D. O. S. 1994, ApJS, 91, 659
Lada C.J., Thronson H. A., Smith H. A., Schwartz, P. R., & Glaccum, W. 1984, ApJ, 286, 302
Lekht, E. E., Likhachev, S. F., Sorochenko, R. L., & Strel'Nitskii, V. S. 1993, ARep, 37, 367L
Lekht, E. E., & Sorochenko, R. L. 2001, ARep, 45, 113L
Lucas, R., Le Squéren, A., Kazès, I., & Encrenaz, P. J. 1978, A&A, 66, 155
Maisel, L. 1971, Probability, Statistics, and Random Processes (Simon and Schuster), 54
Migenes, V., Cohen, R. J., & Brebner, G. C. 1992, MNRAS, 254, 501
Migenes, V., Horiuchi, S., Slysh, V. I., et al. 1999, ApJS, 123, 487
Miralles, M. P., Rodríguez, L. F., & Scalise, E. 1994, ApJS, 92, 173
Mitchell, G. F., Maillard J., & Hasewaga T. I. 1991, ApJ, 371, 342
Moscadelli, L., Cesaroni, R., & Rioja, M. J. 2000, A&A, 360, 663
Palagi, F., Cesaroni, R., Comoretto, G., Felli, M., & Natale, V. 1993, A&AS, 101, 153
Patel, N. A., Greenhill, L. J., Herrnstein, J., Zhang, Q., Moran, J. M., Ho, P. T. P., & Goldsmith, P. F. 2000, ApJ, 538, 268
Persi, P., Palagi, F., & Felli, M. 1994, A&A, 291, 577
Reid, M. J., & Moran, J. M. 1981, ARA&A, 19, 231
Richer, J., Padman, R., Ward-Thompson, D., Hills, R. E., & Harris, A. I. 1993, MNRAS, 262, 839
Roberts, W. W. 1972, ApJ, 173, 259
Rodríguez, L. F., & Cantó, J. 1983, RevMexAA, 8, 163
Rodríguez, L. F., Haschick, A. D., Torrelles, J. M., & Myers, P. C. 1987, A&A, 186, 319
Rodríguez, L. F., Moran, J. M., Gottlieb, E. W., & Ho, P. T. P. 1980, ApJ, 235, 845
Schwartz, P. R. 1989, ApJ, 338, L25
Seth, A. C., Greenhill, L. J., & Holder, B. P. 2002, ApJ, 581, 325
Snell, R. L., Dickman, R. L., & Huang, Y. L. 1990, ApJ, 352, 139
Snell, R. L, Huang, Y.-L., Dickman, R. L., & Claussen, M. J. 1988, ApJ, 325, 853
Staude, H. J., Lenzen, R., Dyck, H. M., & Schmidt, G. D. 1982, ApJ, 255, 95
Szymczak, M., Hrynek, G., & Kus, A. J. 2000, A&AS, 143, 269
Tofani, G., Felli, M., Taylo,r G. B., & Hunter, T. R. 1995, A&AS, 112, 299
Torrelles, J. M., Gómez, J. F., Anglada, G., Estalella, R., Mauersberger, R., & Eiroa, C. 1992, ApJ, 392, 616
Torrelles, J. M., Gómez, J. F., Rodríguez, L. F., Curiel, S., Ho, P. T. P., & Garay, G. 1996, ApJ, 457, L107
Torrelles, J. M., Patel, N. A., Gómez, J. F., Ho, P. T. P., Rodríguez, L. F., Anglada, G., Garay, G., Greenhill, L., Curiel, S., & Cantó, J. 2001, Nature, 411, 277
Torrelles, J. M., Rodríguez, L. F., Cantó, J., Marcaide, J., & Gyulbudaghian, A. L. 1983, RevMexAA, 8, 147
Torrelles, J. M., Patel, N. A., Gómez, J. F., Ho, P. T. P., Rodríguez, L. F., Anglada, G., Garay, G., Greenhill, L., Curiel, S., & Cantó, J. 2001, Nature, 411, 277
Trinidad, M. A., Curiel, S., Cantó, J., D'Alessio, P., Torrelles, J. M., Rodríguez, L. F., Gómez, J. F., Ho. P. T. P., & Patel, N. 2003a, ApJ, 589, 386
Trinidad, M. A., Curiel, S., Cantó, J., Torrelles, J. M., Rodríguez, L. F., Gómez, J. F., Ho. P. T. P., & Patel, N. 2003b, in preparation
Valdettaro, R., Palla, F., Brand, J., Cesaroni, R., Comoretto, G., Di Franco, S., Felli, M., Natale, E., Palagi, F., Panella, D., and Tofani, G. 2001, A&A, 368, 845
Valdettaro, R., Palla, F., Brand, J., Cesaroni, R., Comoretto, G., Felli, M., & Palagi, F. 2002, A&A, 383, 244
Wilking, B. A., Blackwell, J. H., & Mundy, L. G. 1990, AJ, 100, 758

Wilking, B. A., Mundy, L. G., Blackwell, J. H., & Howe, J. E. 1989, ApJ, 345, 257
Wood, D. O. S., & Churchwell, E. 1989, ApJ, 340, 265
Wootten, A. 1993, Proceedings of Local Conference, Astrophysical Masers, Arlington, VA, USA (1992), 412, 315
Wouterloot, J. G. A., Brand, J., & Fiegle, K. 1993, A&AS 98, 589
Wouterloot, J. G. A., Henkel, C., & Walmsley, C. M. 1989, A&A, 215, 131

Salvador Curiel, Victoria Rojas, and Miguel Angel Trinidad: Instituto de Astronomía, UNAM, Apdo. Postal 70-264, 04510 México D. F., México (trinidad@astroscu.unam.mx).
Juan Carlos Plascencia and Luis F. Rodríguez: Centro de Astronomía y Astrofísica, UNAM, Apdo. Postal 3-72, 58090 Morelia, Michoacán, México (l.rodriguez@astrosmo.unam.mx).